Journal of Advanced Ceramics
2014, 3(1): 49–55
DOI: 10.1007/s40145-014-0092-2

ISSN 2226-4108
CN 10-1154/TQ

Research Article

Structure and composition study of carbon-doped titanium oxide film combined with first principles

Wei MAI[a], Feng WEN[a,*], Dong XIE[b], Yongxiang LENG[b], Zhonglin MU[c]

[a]*Key Lab of Advanced Materials of Tropical Island Resources of Ministry of Education*, *School of Materials and Chemical Engineering*, *Hainan University*, *Haikou 570228*, *P.R.China*
[b]*Key Lab of Advanced Technologies of Materials*, *Ministry of Education*, *Chengdu 610031*, *P.R.China*
[c]*Hainan Medical University*, *Haikou 571199*, *P.R.China*

Received: October 23, 2013; Revised: January 04, 2014; Accepted: January 08, 2014

Abstract: Carbon-doped titanium oxide (C/Ti–O) films were prepared on Si(100) wafer, stainless steel (type 304) and glass by reactive magnetron sputtering (RMS) using CO_2 gas as carbon and oxygen source under room temperature (RT). X-ray diffraction (XRD) and X-ray photoelectron spectroscopy (XPS) were used to analyze structure and composition of the as-prepared C/Ti–O film. It could be observed from XRD that the as-prepared C/Ti–O film contained TiO crystal phase structure. Ti2p XPS spectrum of the as-prepared C/Ti–O film showed that the valences of titanium were made up of Ti^{2+}, Ti^{3+} and Ti^{4+}. C1s XPS spectrum revealed that carbon was doped into titanium oxide based on the existence of the typical Ti–C bond. The optical absorption curve by ultraviolet–visible (UV–Vis) spectrophotometer showed that the C/Ti–O film appeared the remarkable red shift of absorption edge, which contributed to C substitution in O sites in amorphous TiO_2. Photocatalysis test using methyl orange (MO) as indicator confirmed that the as-prepared C/Ti–O film had photocatalytic activity. Combined with the results of the tests and first-principles calculations, a potential photocatalysis mechanism was proposed.

Keywords: C/Ti–O films; carbon-doped; magnetron sputtering; first principles

1 Introduction

TiO_2 as a promising semiconductor material has received intense attention for environmental cleaning, water splitting and solar cells due to its low cost, nontoxicity, long-term stability and high oxidative power [1–3]. However, TiO_2 used as photocatalyst shows photoactivity only under ultraviolet (UV) light due to its large intrinsic energy band gap (E_g = 3.2 eV) [4]. Furthermore, the recombination of photo-generated electron–hole pair is relatively easy in TiO_2. Therefore, many attempts have been made to improve the photocatalytic efficiency of TiO_2 in order to overcome the UV limitation and extend the optical absorption of TiO_2 to the visible-light region, involving doping other chemical elements [5,6], semiconductor compounding [7] and dye sensitizing [8].

As a result, nonmetal doping, such as N [9], C [10], F [11], S and P [12], has been extensively investigated. Wang *et al*. [13] prepared a C-doped TiO_2 catalyst

* Corresponding author.
E-mail: fwen323@163.com

using a nonhydrolytic sol–gel method and found that substitutional and interstitial carbon atoms coexist in the lattice of TiO_2. Yang *et al*. [14] found the surface area of the C and N co-doped TiO_2-based photocatalyst is increased, and the photocatalytic efficiency is enhanced. Unfortunately, the previous modification studies were based on crystalline TiO_2, and little attention has been paid to amorphous TiO_2 because it is commonly accepted that amorphous TiO_2 contains high concentration of defects, which can function as rapid electron–hole pair recombination centers rendering them inactive [15]. Hence, there have been only few studies and reports of amorphous TiO_2 [16–19], especially amorphous TiO_2 with TiO crystal phase.

In this study, carbon-doped titanium oxide (C/Ti–O) films were synthesized by reactive magnetron sputtering (RMS) using CO_2 as carbon and oxygen source under room temperature (RT). Structure and composition of the C/Ti–O film were studied by the analysis of X-ray diffraction (XRD) and X-ray photoelectron spectroscopy (XPS). Optical absorption characteristic of the C/Ti–O film was measured by UV–Vis spectrophotometer. Combined with first-principles calculations, the potential photocatalysis mechanism of the C/Ti–O film was proposed.

2 Experiment

2.1 Film preparation and characterization

The C/Ti–O films were prepared on Si(100) wafer and stainless steel (type 304) by RMS, discharging Ar and CO_2 gas mixture (the ratio of Ar/CO_2 was 60 sccm to 18 sccm) and using high-purity titanium (99.99%) as titanium plasma source under RT. The C/Ti–O film was also prepared on glass for absorbance measurement.

The microstructure of the C/Ti–O film was measured by XRD (X'Pert Pro MPD, Philips, the Netherlands) using glancing diffraction method with an incident angle of $\theta = 0.5°$. The chemical composition of the C/Ti–O film was determined using XPS (Type K-ALPHA, Thermo Electron Corporation, USA). Absorbance is a very important property for assessing photocatalysis. The absorbance of the as-prepared C/Ti–O film was measured by UV–Vis spectrophotometer (type TU-1810) in the wavelength range of 250–900 nm.

Photocatalytic activity of the C/Ti–O film was also evaluated by the degradation test of methyl orange (MO) under UV light irradiation. During the photo-degradation test, the C/Ti–O film was placed into the MO solution (10 mg/L) loaded in a dish. A 15-W bactericidal lamp as UV source was placed on the top of the dish with the spacing between the light bulb and the surface of the dish being 34 cm. The concentration of MO in solution was measured during an interval of time by monitoring the absorbance at 464 nm on the UV–Vis spectrophotometer. The degradation of reactant could be calculated by

$$\eta(\%) = \frac{c_0 - c}{c_0} \times 100 \quad (1)$$

where c_0 is the initial concentration of MO; c is the concentration of MO after t-min irradiation.

2.2 Models and methods of calculation

Figure 1 shows the supercell structures of crystalline

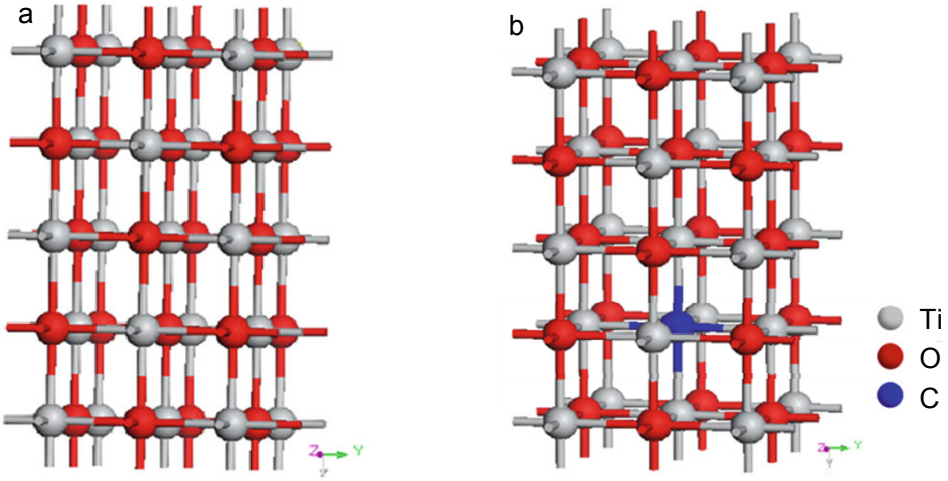

Fig. 1 The supercell structures of (a) TiO and (b) C-doped TiO.

TiO (TiO) and C-doped TiO, respectively. TiO has a body-centered cubic structure with $a = 4.1766$ Å [20]. Supercells built of 2×1×1 unit cells were used in the calculations for undoped (Fig. 1(a)) and substitutional doped systems (Fig. 1(b)). For the C-doped TiO model, an O atom (0.25, 0.50, 0.50) was replaced by a C atom. The units of pure TiO and C-doped TiO were optimized employing the CASTEP module of Materials Studio 5.0 developed by Accelrys. The total plane-wave pseudopotential method forms the basis of the CASTEP calculations. The electronic exchange correlation energy was treated under the generalized gradient approximation (GGA) with the Perdew–Burke–Ernzerhof method. The plane-wave based cut-off energy was set at 340 for TiO and C-doped TiO. The Monkhorst–Packschemek point grid sampling was set at 7×7×7 for the Brillouin zone. All convergence parameters were set as follows: total energy tolerance of 1.0×10^{-5} eV/atom, maximum force tolerance of 0.03 eV/nm and maximum stress component of 0.05 GPa. After geometry optimization, band structure, total density of states (DOS) and partial density of states (PDOS) were calculated.

3 Results and discussion

3.1 Microstructure

Figure 2 is the XRD pattern of the as-prepared C/Ti–O film on Si(100) wafer. In Fig. 2, the diffraction peaks corresponding to (100), (200), (220), (311) and (222) crystal planes of TiO are observed. The small-angle X-ray scattering (SAXS) pattern matches well with the standard powder diffraction data (JCPDS No. 08-0117). Zhang *et al*. [21] and Martin *et al*. [22] found that the anatase and rutile phases coexist in the films when a target of titanium (99.995%) and a mixture of argon and oxygen gases are used to deposit TiO_2 films on Si(100) wafers. However, no observable peak of rutile or anatase TiO_2 is observed in the C/Ti–O film, which indicates the incorporated C in the as-prepared C/Ti–O film inhibits the formation of rutile or anatase phase [23].

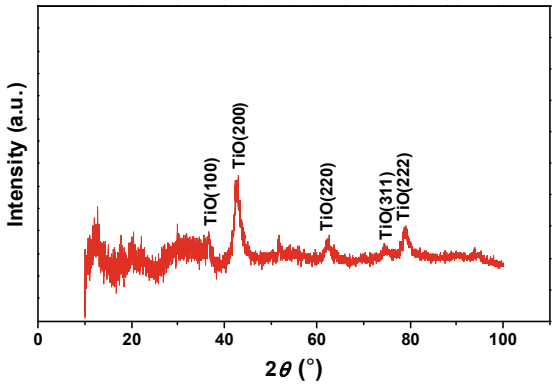

Fig. 2 XRD pattern of the C/Ti–O film in a grazing angle configuration ($\theta = 0.5°$).

3.2 Chemical composition

XPS is quite sensitive to the characteristics of the film surface, because the non-elastic scattering mean free path λ_m of emitted photoelectron is very short [24]. Figure 3 is the C1s and Ti2p XPS spectra of the C/Ti–O film after etching for 30 s in order to eliminate the effect of the surface absorption. The C1s spectrum could be deconvoluted into two peaks by Gaussian fitting and approximating the contribution of background by the smart mode at about 282.0 eV and 284.6 eV as shown in Fig. 3(a). The peak at 284.6 eV is usually attributed to the adventitious carbon or carbon residues from the organic precursor (mainly C–C bond) [25,26]. The additional peak located at 282.0 eV is attributed to the Ti–C bond resulting from the substitution of oxygen atoms by carbon, which indicates carbon is doped into titanium oxide lattice

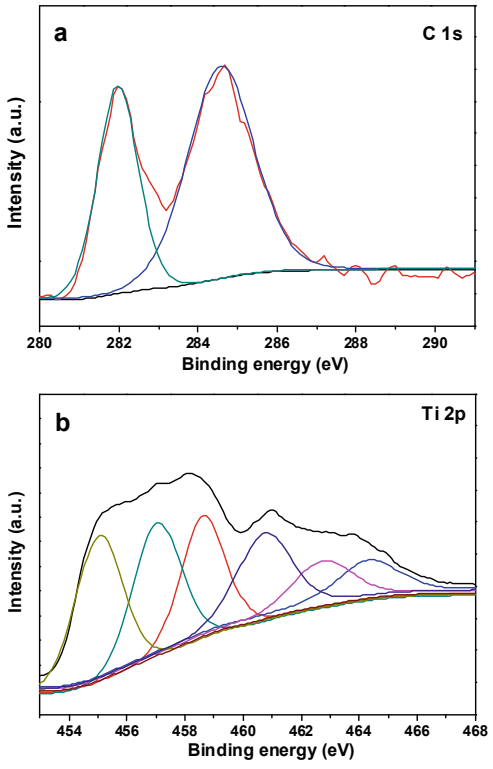

Fig. 3 XPS spectra of amorphous TiO_2 composite: (a) C1s peaks, (b) Ti2p peaks.

successfully. The high-resolution XPS spectrum of Ti2p is illustrated in Fig. 3(b). Ti^{4+} species are indicated by binding energies of 459.3 eV (Ti2p3/2) and 464.6 eV (Ti2p1/2), those of Ti^{3+} species are located at about 456.7 eV (Ti2p3/2) and 462.5 eV (Ti2p1/2), and those of Ti^{2+} species are located at about 455.4 eV (Ti2p3/2) and 461.1 eV (Ti2p1/2) [27]. The binding energy difference

$$\Delta E_b = E_b(\text{Ti2p1/2}) - E_b(\text{Ti2p3/2}) \quad (2)$$

is always close to 5.7 eV, which indicates the standard binding energy for Ti element [28]. Figure 3(b) shows the content of Ti^{4+} and Ti^{3+} is relatively high, but the corresponding crystal structures of Ti^{4+} and Ti^{3+} are not observed in Fig. 2(b), which suggests that amorphous TiO_2 and Ti_2O_3 exist in the as-prepared C/Ti–O film, or the content of TiO_2 and Ti_2O_3 crystal phase is little. Suriye *et al*. [29] reported that TiO_2 surface defects (Ti^{3+}) play significant role as they are active sites for oxygen adsorption and for trapping the electron to prevent the recombination of electrons and holes. Hamdy *et al*. [30] also reported that surface Ti^{3+} sites provide the unique activity and selectivity in the target reactions at relatively high wavelengths. Detailed theoretical explanations are described in Refs. [31,32]. Thus, TiO, amorphous TiO_2 and Ti_2O_3 exist in the as-prepared C/Ti–O film by the analysis of XRD and XPS.

3.3 Absorbance

The optical absorption characteristic of the C/Ti–O film is shown in Fig. 4. The absorbance of P25(TiO_2) is also measured as a comparison as shown in Fig. 4. It could be observed obviously from Fig. 4 that the C/Ti–O film exhibits more remarkable red shift towards visible-light region as compared to P25(TiO_2), which could be attributed to the C2p impurity states created by carbon incorporated into amorphous TiO_2 [33]. To estimate the optical band gap E_g, a Tauc's plot is constructed in which the absorption coefficient A is plotted against the photon energy E as follows:

$$(AE)^{1/2} = B(E - E_g) \quad (3)$$

where B is a proportionality constant. The optical band gap E_g can be deduced from the intercept of the extrapolated straight line with the E axis as shown in Fig. 4(b). The band gap of the C/Ti–O film is only 2.44 eV which is much smaller than the band gap of P25(TiO_2) of 2.95 eV.

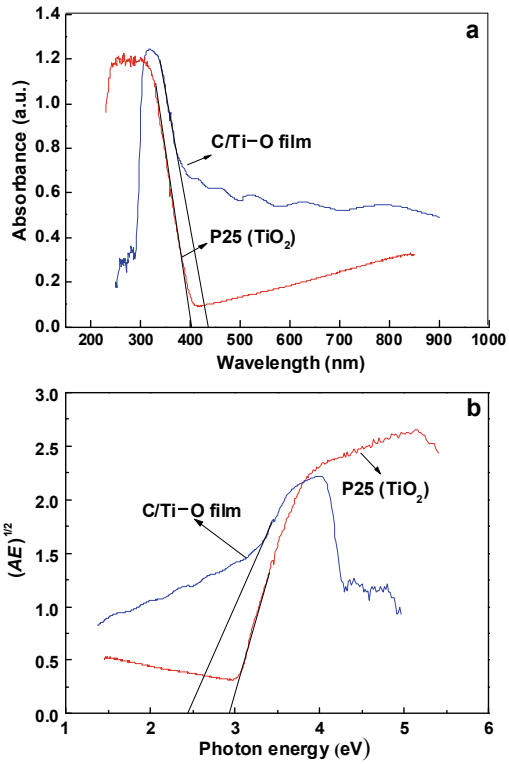

Fig. 4 UV–Vis diffusion reflectance spectra of the C/Ti–O film and P25(TiO_2): (a) absorbance versus wavelength and (b) absorption coefficient versus photo energy.

3.4 Photocatalytic experiment

Figure 5 shows the photoactivity of the C/Ti–O film that is evaluated by heterogeneous degradation of MO waste water under UV irradiation in different time at RT. It is obviously observed that the C/Ti–O film shows some photocatalytic activity. When the C/Ti–O film placed into the MO solution is irradiated for 480

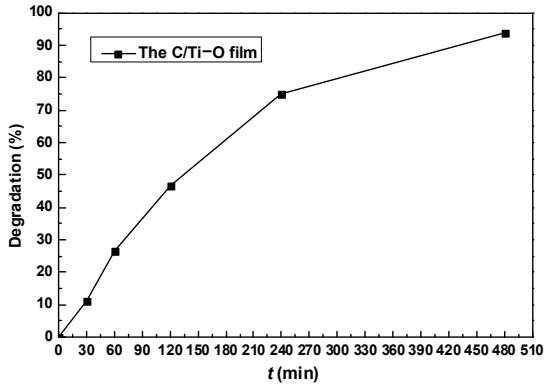

Fig. 5 MO degradation curve using the C/Ti–O film synthesized on stainless steel (type 304) under UV irradiation.

min, the degradation percentage of MO reached to 94%. However, amorphous TiO_2 has long been reported to be nearly inactive due to the facilitated recombination of photo-generated electrons and holes under UV light irradiation [15], which indicates the recombination of photo-generated electrons and holes are restrained. The further explanation is made in the following passage.

3.5 Photocatalysis mechanism

In order to analyze the photocatalysis mechanism of the C/Ti–O film, electronic properties of TiO and C-doped TiO due to TiO crystal phase existed in the as-prepared C/Ti–O film are analyzed using Materials Studio software based on first principles. The calculated energy band structures of the models are showed in Fig. 6. Wang *et al.* [20] reported that TiO is metallic. As shown in Fig. 6(b), approximate parabolic energy levels of the conduction band pass across Fermi level, and the change of the levels has no obvious difference near Fermi level regardless of C doping or not doping, which indicates C-doped TiO is also metallic. As compared to Fig. 6(a), the valence band and conduction band are found to be relatively wider and some impurity levels are only observed near Fermi energy in Fig. 6(b), which implies C-doped TiO could form the new states for shallow impurity levels. To further understand how the band gap changes, the DOS and PDOS of TiO and C-doped TiO models are calculated as shown in Fig. 7. In Fig. 7(b), the conduction band and valence band of C-doped TiO are mainly dominated by the Ti3d and O2p orbitals near Fermi level, respectively. And the states across the Fermi energy are mostly Ti3d states, which are consistent with those of TiO. Hence, C-doped TiO is metallic. In addition, it is found that there is the overlap of Ti3d states and a small amount of C2p states, which contributes to the impurity levels.

Figure 8 gives the potential photocatalysis mechanism of the as-prepared C/Ti-O film with TiO crystal phase under visible-light irradiation. On one hand, C-doping makes the band gap of amorphous TiO_2 decrease and appear the red shift of absorption edge. On the other hand, C-doped TiO as metal load of amorphous TiO_2 surface participates in transferring the photoproduction electronics from the CB of C-doped TiO_2 [34]. This phenomenon benefits the separation of electrons and holes. Hence, the C/Ti–O film with TiO crystal phase has the photocatalytic activity.

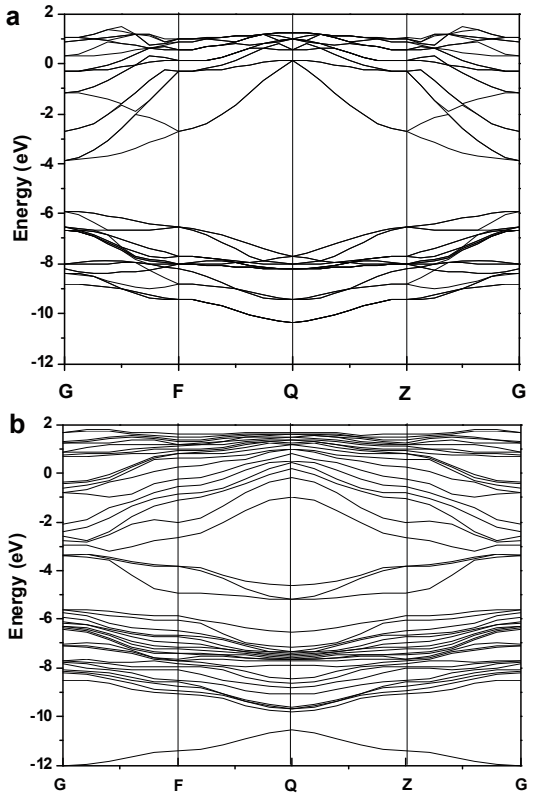

Fig. 6 Calculated band structures for (a) TiO and (b) C-doped TiO.

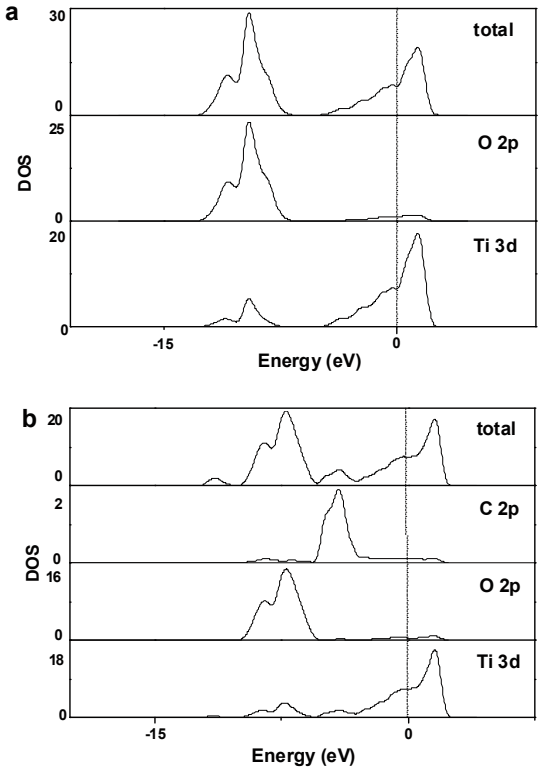

Fig. 7 DOS and PDOS for (a) TiO and (b) C-doped TiO.

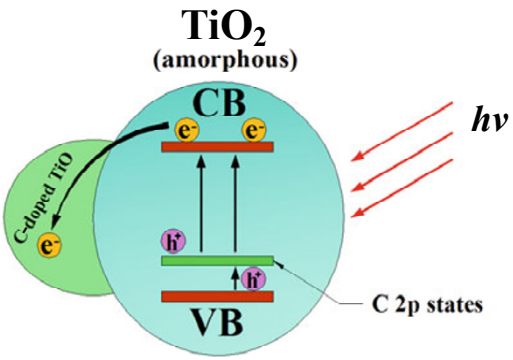

Fig. 8 Photocatalysis mechanism of the as-prepared C/Ti–O film under visible-light irradiation

4 Conclusions

In this paper, the C/Ti–O film was prepared by RMS using CO_2 gas as carbon and oxygen source. It was confirmed that C was doped into titanium oxide successfully based on the existence of the typical Ti–C bond. The as-prepared C/Ti–O film showed the red shift of absorption edge compared with P25(TiO_2), which contributed to C substitution in O sites in amorphous TiO_2. Secondly, C-doped TiO as metal load was confirmed using Materials Studio software based on first principles, which benefitted the separation of electrons and holes and made the C/Ti–O film with TiO crystal phase exhibit photocatalytic activity.

Acknowledgements

This work was financially supported by the National Natural Science Foundation of China (Nos. 51062002 and 81171462), National Science Fund of Hainan Province (No. 511113) and Key Project of Science and Technology Planning of Hainan Province (No. ZDXM20110051).

References

[1] Linsebigler AL, Lu G, Yates JT. Photocatalysis on TiO_2 surfaces: Principles, mechanisms, and selected results. *Chem Rev* 1995, **95**: 735–758.

[2] Azevedo EB, Neto FRA, Dezotti M. TiO_2-photocatalyzed degradation of phenol in saline media: Lumped kinetics, intermediates, and acute toxicity. *Appl Catal B*: *Environ* 2004, **54**: 165–173.

[3] Baran W, Makowski A, Wardas W. The effect of UV radiation absorption of cationic and anionic dye solutions on their photocatalytic degradation in the presence TiO_2. *Dyes Pigments* 2008, **76**: 226–230.

[4] Hashimoto K, Irie H, Fujishima A. TiO_2 photocatalysis: A historical overview and future prospects. *Jpn J Appl Phys* 2005, **44**: 8269–8285.

[5] Hung W-C, Fu S-H, Tseng J-J, *et al*. Study on photocatalytic degradation of gaseous dichloromethane using pure and iron ion-doped TiO_2 prepared by the sol–gel method. *Chemosphere* 2007, **66**: 2142–2151.

[6] Li M, Zhang J, Guo D, *et al*. Band gap engineering of compensated (N, H) and (C, 2H) codoped anatase TiO_2: A first-principles calculation. *Chem Phys Lett* 2012, **539–540**: 175–179.

[7] Fujii H, Inata K, Ohtaki M, *et al*. Synthesis of TiO_2/CdS nanocomposite via TiO_2 coating on CdS nanoparticles by compartmentalized hydrolysis of Ti alkoxide. *J Mater Sci* 2001, **36**: 527–532.

[8] Otaka H, Kira M, Yano K, *et al*. Multi-colored dye-sensitized solar cells. *J Photoch Photobio A* 2004, **164**: 67–73.

[9] In S, Orlov A, Berg R, *et al*. Effective visible light-activated B-doped and B, N-codoped TiO_2 photocatalysts. *J Am Chem Soc* 2007, **129**: 13790–13791.

[10] Lee J-Y, Park J, Cho J-H. Electronic properties of N- and C-doped TiO_2. *Appl Phys Lett* 2005, **87**: 011904.

[11] Yu Y, Wu H-H, Zhu B-L, *et al*. Preparation, characterization and photocatalytic activities of F-doped TiO_2 nanotubes. *Catal Lett* 2008, **121**: 165–171.

[12] Yang K, Dai Y, Huang B. Understanding photocatalytic activity of S- and P-doped TiO_2 under visible light from first-principles. *J Phys Chem C* 2007, **111**: 18985–18994.

[13] Wang X, Meng S, Zhang X, *et al*. Multi-type carbon doping of TiO_2 photocatalyst. *Chem Phys Lett* 2007, **444**: 292–296.

[14] Yang X, Cao C, Erickson L, *et al*. Synthesis of visible-light-active TiO_2-based photocatalysts by carbon and nitrogen doping. *J Catal* 2008, **260**: 128–133.

[15] Ohtani B, Ogawa Y, Nishimoto S. Photocatalytic activity of amorphous-anatase mixture of titanium(IV) oxide particles suspended in aqueous solutions. *J Phys Chem B* 1997, **101**: 3746–3752.

[16] Randorn C, Wongnawa S, Boonsin P. Bleaching of

methylene blue by hydrated titanium dioxide. *ScienceAsia* 2004, **30**: 149–156.

[17] Zhang Z, Maggard PA. Investigation of photocatalytically-active hydrated forms of amorphous titania, $TiO_2{\cdot}nH_2O$. *J Photoch Photobio A* 2007, **186**: 8–13.

[18] Li J, Liu S, He Y, *et al*. Adsorption and degradation of the cationic dyes over Co doped amorphous mesoporous titania–silica catalyst under UV and visible light irradiation. *Microporous Mesoporous Mater* 2008, **115**: 416–425.

[19] Kanna M, Wongnawa S, Buddee S, *et al*. Amorphous titanium dioxide: A recyclable dye remover for water treatment. *J Sol–Gel Sci Technol* 2010, **53**: 162–170.

[20] Wang H, Zong Z, Yan Y, *et al*. First-principles study of ferromagnetism in N doped TiO_2 and TiO. *J Magn Magn Mater* 2012, **324**: 2858–2860.

[21] Zhang Y, Ma X, Chen P, *et al*. Effect of the substrate temperature on the crystallization of TiO_2 films prepared by DC reactive magnetron sputtering. *J Cryst Growth* 2007, **300**: 551–554.

[22] Martin N, Santo AME, Sanjinés R, *et al*. Energy distribution of ions bombarding TiO_2 thin films during sputter deposition. *Surf Coat Technol* 2001, **138**: 77–83.

[23] Dang BHQ, Rahman M, MacElroy D, *et al*. Evaluation of microwave plasma oxidation treatments for the fabrication of photoactive un-doped and carbon-doped TiO_2 coatings. *Surf Coat Technol* 2012, **206**: 4113–4118.

[24] Cong Y, Li X, Qin Y, *et al*. Carbon-doped TiO_2 coating on multiwalled carbon nanotubes with higher visible light photocatalytic activity. *Appl Catal B*: *Environ* 2011, **107**: 128–134.

[25] Gu D, Lu Y, Yang B, *et al*. Facile preparation of micro–mesoporous carbon-doped TiO_2 photocatalysts with anatase crystalline walls under template-free condition. *Chem Commun* 2008: 2453–2455.

[26] Yang J, Bai H, Jiang Q, *et al*. Visible-light photocatalysis in nitrogen–carbon-doped TiO_2 films obtained by heating TiO_2 gel–film in an ionized N_2 gas. *Thin Solid Films* 2008, **516**: 1736–1742.

[27] Fu Y, Du H, Zhang S, *et al*. XPS characterization of surface and interfacial structure of sputtered TiNi films on Si substrate. *Mat Sci Eng A* 2005, **403**: 25–31.

[28] Yang J, Dai J, Li J. Synthesis, characterization and degradation of Bisphenol A using Pr, N co-doped TiO_2 with highly visible light activity. *Appl Surf Sci* 2011, **257**: 8965–8973.

[29] Suriye K, Praserthdam P, Jongsomjit B. Control of Ti^{3+} surface defect on TiO_2 nanocrystal using various calcination atmospheres as the first step for surface defect creation and its application in photocatalysis. *Appl Surf Sci* 2007, **253**: 3849–3855.

[30] Hamdy MS, Amrollahi R, Mul G. Surface Ti^{3+} containing (blue) titania: A unique photocatalyst with high activity and selectivity in visible light-stimulated selective oxidation. *ACS Catal* 2012, **2**: 2641–2647.

[31] Kubokawa Y, Anpo M, Yun C. Olefin photooxidation and oxygen anion radicals on oxide surfaces. *Stud Surf Sci Catal* 1981, **7**: 1170–1184.

[32] Anpo M, Chiba K, Tomonari M, *et al*. Photocatalysis on native and platinum-loaded TiO_2 and ZnO catalysts. Origin of different reactivities on wet and dry metal oxides. *B Chem Soc Jpn* 1991, **64**: 543–551.

[33] Gao H, Ding C, Dai D. Density functional characterization of C-doped anatase TiO_2 with different oxidation state. *J Mol Struc-THEOCHEM* 2010, **944**: 156–162.

[34] Li F, Zhao Y, Hao Y, *et al*. N-doped P25 TiO_2–amorphous Al_2O_3 composites: One-step solution combustion preparation and enhanced visible-light photocatalytic activity. *J Hazard Mater* 2012, **239–240**: 118–127.